JOURNAL OF MATERIALS SCIENCE 23 (1988) 1351–1359

Room-temperature forming limit diagram and tensile behaviour up to 200° C of an Al–Ca–Zn superplastic alloy

P. P. DATE, K. SWAMINATHAN, K. A. PADMANABHAN
Department of Metallurgical Engineering, Indian Institute of Technology, Madras 600 036, India

The forming limit diagram and strain distribution under punch stretching at room temperature of an Al–Ca–Zn (superplastic) alloy have been evaluated. Tensile behaviour up to 200° C is reported. The fracture surfaces have been examined by scanning electron microscopy and the results are analysed to support the failure criterion proposed earlier by Marciniak *et al.*

1. Introduction

Moore and Morris [1] have reported structurally superplastic flow in an Al–Ca–Zn alloy. However, the low-temperature (ambient and up to 200° C) properties of this alloy, having a microstructure conducive to superplasticity, are not known.

In this paper, the forming limit diagram (FLD) of the Al–Ca–Zn alloy at room temperature is determined using the method reported by Keeler and Backofen [2] and Hecker [3]. Strain distribution in punch stretching is evaluated. Tensile properties up to 200° C are reported. Fractography was used to account for the differences in behaviour under various testing conditions. The fracture criterion of Marciniak *et al.* [4, 5] is verified.

2. Experimental procedure

Sheets of the alloy, 1 mm thick, were supplied by the Alcan Research Laboratories, Canada. The composition (wt %) was Ca 4.87, Zn 4.64, Fe 0.13, Si 0.09, Mg 0.01, Al balance.

When subjected to punch stretching, the as-received material shattered. To obtain a microstructure similar to that present during superplastic flow, the as-received material was soaked at 540° C for 30 min and air cooled [6]. The two-dimensional grain size of the second phase was 2.0 ± 0.5 μm. The matrix grains could not be fully revealed. As in an earlier study [1], the isolated grains that were visible had a size equal to that of the second phase. Blanks for FLD measurements and tensile specimens were cut from these sheets.

2.1. Determination of FLD

Blanks of constant length 100 mm, and varying widths of 100, 80, 70, 60, 50, 40, 25 and 15 mm were cut, with the length always perpendicular to the sheet rolling direction. This enabled the determination of the transverse FLD of the sheet, which is standard practice [3]. Using a screen printing process, the blanks were gridded with non-contacting circles of 2.5 mm diameter. Each blank was clamped securely by a circular draw bead of 60 mm diameter on a double-action hydraulic press and stretched over a hemispherical punch of 25 mm diameter at an average speed of 10 mm min^{-1}. The hold-down pressure was in the range of 1.03 MPa (10 atm).

To obtain a number of strain ratios, several specimens were tested for each width. Some tests were stopped at visible necking; others continued until fracture.

The grid circles became ellipses on deformation. The major and minor axes of the ellipses were measured using a travelling microscope, with a least count of ± 0.01 mm at a magnification of × 10. The major and minor engineering strains were computed and plotted against each other. The strain distribution in blanks of different widths was also measured along a longitudinal traverse.

2.2. Tensile testing

To obtain the largest negative minor strains in the FLD, tensile specimens of dimensions 50 mm gauge length, 12.5 mm width, 1 mm thickness and with the axis perpendicular to the sheet rolling direction were screen printed with non-contacting circles of 2.5 mm diameter. These specimens were tested to fracture at room temperature on an Instron machine at a cross-head speed of 10 mm min^{-1}. Major and minor strains were calculated, as before.

Tensile specimens with the axis parallel to rolling direction and dimensions 16 mm × 4 mm × 1 mm (gauge portion), were pulled to fracture on an Instron machine employing different cross-head speeds (0.5, 2, 5, 10 mm min^{-1}) and temperatures (25, 80, 130, 190° C). The strain-rate sensitivity index, m, was determined at room temperature and 250° C using the strain-rate change tests [7].

2.3. Fractography

The fracture surfaces resulting from the punch stretching of blanks as well as tensile testing were examined in a scanning electron microscope.

0022–2461/88 $03.00 + .12

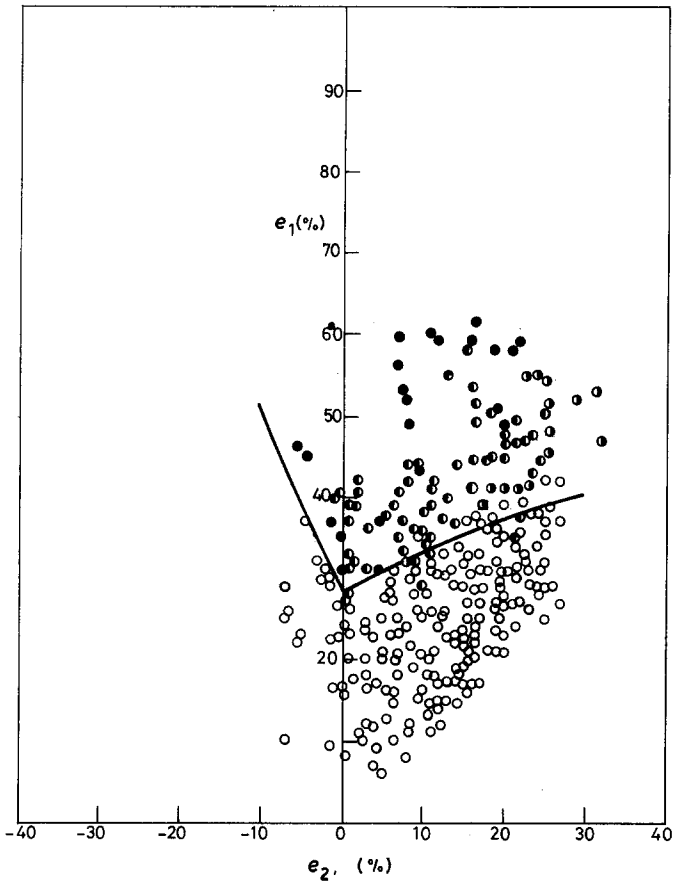

Figure 1 The room-temperature forming limit diagram of the Al–Ca–Zn alloy. (○) Safe ellipses, (◐) necked ellipses, (●) failed ellipses.

3. Results

3.1. Forming limit diagram

The FLD is shown in Fig. 1. Ductility was greater in biaxial tension than when drawing was dominant. The largest major strain of 40% was seen, when the minor strain was 30%. A plane strain of 27% and a maximum negative strain of about 8% were also recorded.

3.2. Strain distribution

The distribution of strain across blanks of different widths is shown in Figs 2a to h. For large blank widths (> 60 mm), the major and minor strains at the pole were nearly equal. For smaller widths, the two strains differed significantly. The type of distribution of minor strain above and below a blank width of 60 mm was also different. The distribution of major strain, however, followed the same pattern at all widths.

3.3. Tensile properties

Some important properties, along with the values of K and n in the equation $\sigma = K\varepsilon^n$ where σ is the true stress, ε the true strain, n the strain-hardening index and K a material constant, used to analyse plastic flow in the material, are given in Table I. (In the temperature range employed, the strain-rate sensitivity index, m, was only of the order of 0.005 to 0.09. Thus, the approximation of the equation $\sigma = K^*\varepsilon^n\dot{\varepsilon}^m$, where $\dot{\varepsilon}$ is the strain rate, to $\sigma = K\varepsilon^n$ does not introduce serious errors.) The variations in the uniform, total and post-uniform strains with the experimental conditions are shown in Fig. 3.

With increasing temperature, the uniform strain, n, and the strain-rate dependence of ductility decreased. However, a direct relationship existed between the post-uniform strain and temperature. In general, n went through a maximum with strain rate, but at 80° C, n was virtually independent of strain rate. The changes in the value of K with strain rate and temperature, on the other hand, fell within a narrow band (Table I).

The strain-rate sensitivity index, m, deduced from the relation (at constant strain) of $\sigma \propto \dot{\varepsilon}^m$ rose from 0.005 at room temperature to 0.09 at 250° C.

3.4. Fractography

Tensile fracture was concentrated upon because it revealed some interesting features. This was not the case with fracture surfaces resulting from punch stretching, which were somewhat similar.

3.4.1. Fracture in punch stretched specimens

Here the fracture surfaces appeared similar and Table II shows that even the dimple size did not change appreciably with a change in the width of the blank.

3.4.2. Tensile Fracture

The macrographs shown in Figs 4a and b, correspond to different strain rates at 25° C. The appearance is rugged and similar, indicative of comparable (low) ductility. Fig. 4c, corresponding to a higher temperature, reveals a smoother surface and a greater reduction in area, characteristic of higher ductility.

Figs 5a to d (taken at × 1000) correspond to different temperatures, but the same strain rate of deformation. Table III gives the relationship between the test temperature, dimple size and ductility.

Isolated dimples were nearly spherical in shape. With increasing ductility, the dimples inter-linked and acquired an oblong shape. This resulted in (a) clumps of grains becoming surrounded by cavities on all sides

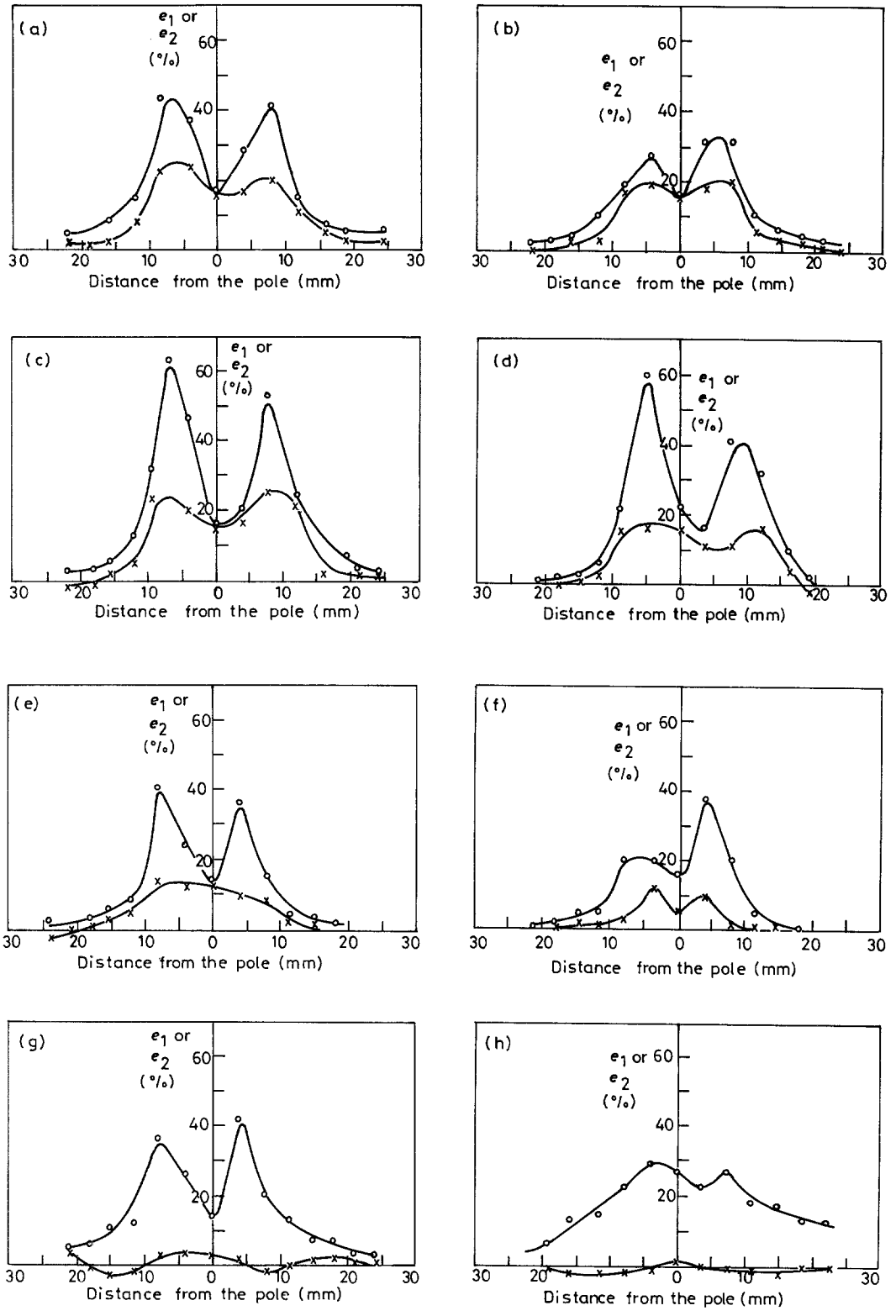

Figure 2 Distribution of major and minor strains in blanks of different widths. Longitudinal traverse: (a) 100 mm, (b) 80 mm, (c) 70 mm, (d) 60 mm, (e) 50 mm, (f) 40 mm, (g) 25 mm, (h) 15 mm. (○) e_1, (×) e_2.

and pulling out, and/or (b) an alignment of the dimples in the direction of the stress. At all temperatures, tear ridges connected the different fracture paths produced by the linking of cavities (dimples). The following correlations could be established: (i) ductility increased with an increase in dimple size, and (ii) the width of the tear ridges decreased with increasing ductility.

At higher temperatures, e.g. 190° C, grain-boundary sliding was present (Fig. 6).

The specimens were also examined at higher magnifications of × 1500 and × 3000. These pictures are not presented because the details were similar.

A feature common to both the punch stretching and tension experiments, was the presence of shear facets due to inclusions [6]. Fig. 7 is an example.

4. Discussion

4.1. Forming limit diagram

The presence of low negative strains, even in uniaxial tension, indicates a low r value, where r is the ratio of the width strain to thickness strain. This is

TABLE I Mechanical properties of the Al–Ca–Zn alloy in the range 25 to 190° C

Serial no.	Temperature (° C)	Cross-head speed (mm min^{-1})	Initial upper yield point (MPa)	Lower yield point (MPa)	Yield point elongation (mm)	Ultimate tensile strength (MPa)	Uniform elongation (mm)	Post-uniform elongation (mm)	Total elongation (mm)	n	K (MPa)
1	190	0.5	99.8	–	–	–	–	–	3.70	0.06	102.3
2	190	2.0	115.0	104.5	1.20	105.7	1.85	2.60	4.45	0.11	144.5
3	190	5.0	126.6	117.6	1.12	115.9	1.74	2.34	4.68	0.13	136.5
4	190	10.0	133.0	119.5	0.84	121.4	2.04	2.30	4.34	0.13	168.0
5	130	0.5	130.0	125.9	0.93	129.7	2.10	1.64	3.74	0.11	195.0
6	130	2.0	140.6	133.0	1.02	139.0	2.12	1.87	3.99	0.12	199.5
7	130	5.0	141.3	131.1	1.09	137.8	2.64	1.44	4.08	0.14	218.8
8	130	10.0	149.6	126.8	0.89	147.3	2.29	0.94	3.23	0.15	251.2
9	80	0.5	159.1	132.3	0.76	169.1	2.25	1.19	3.44	0.14	257.0
10	80	2.0	143.7	140.1	0.65	159.1	2.79	0.98	3.77	0.14	281.8
11	80	5.0	143.0	115.4	0.44	159.1	2.54	0.84	3.38	0.15	251.2
12	80	10.0	141.3	139.0	0.61	155.6	2.54	0.72	3.26	0.14	223.9
13	25	0.5	112.8	–	0.44	146.0	2.64	0.55	3.19	0.14	213.8
14	25	2.0	111.6	109.3	0.40	142.5	2.78	0.44	3.22	0.17	240.0
15	25	5.0	162.7	161.5	0.37	190.3	2.67	0.83	3.50	0.17	302.0
16	25	10.0	118.8	112.8	0.35	147.5	2.69	1.08	3.77	0.16	240.0

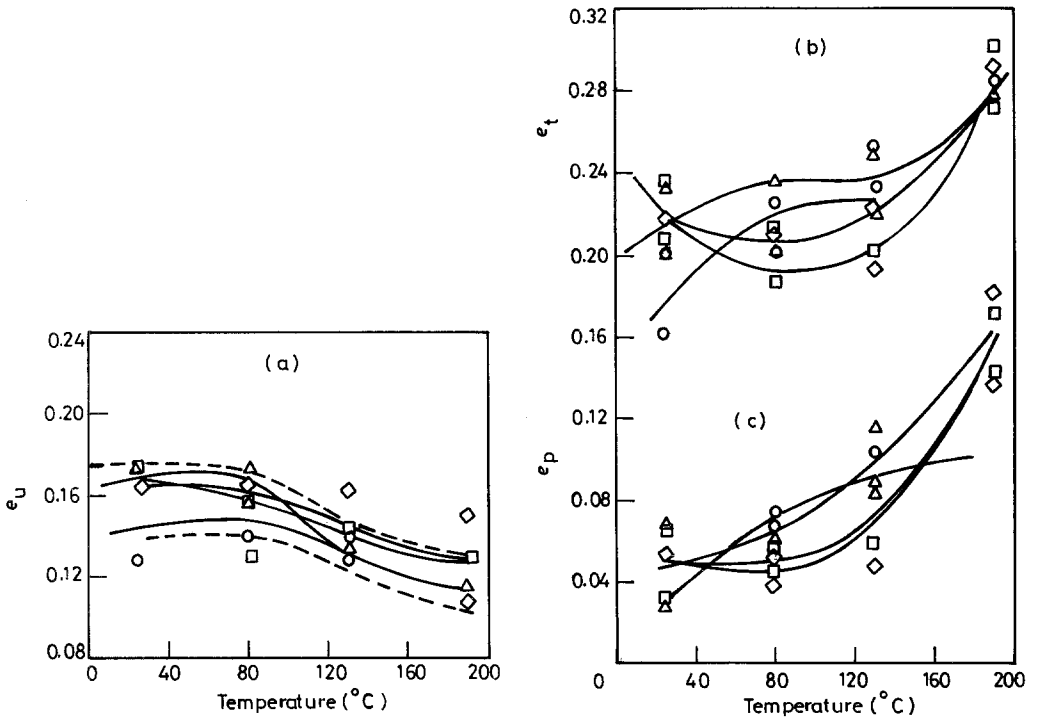

Figure 3 The effect of temperature and cross-head speed on (a) uniform, (b) total and (c) post-uniform strains. Tension tests. (○) 0.5 mm min^{-1}, (△) 2.0 mm min^{-1}, (◇) 5.0 mm min^{-1}, (□) 10.0 mm min^{-1}.

understandable because for materials with a microstructure conducive to superplasticity, r is relatively low [7]. A reasonably high value of n, on the other hand, ensures somewhat better ductility in biaxial stretching. In this study, hydraulic bulging ($e_1 = e_2$, where e_1 and e_2 are the major and minor engineering strains) was not generally present, perhaps due to the presence of friction and some lateral drawing. Other contributory causes could have been the lack of true sphericity in the punch, slight tool misalignment and/or absence of exact centring of the blank. Nevertheless, beyond a blank width of about 80 mm, equi-biaxial tension was present at the pole.

With decreasing blank width (i.e. below 60 mm diameter of the draw bead), the stretching force in the e_2 direction decreases (due to inferior gripping) and the minor strain at the pole progressively falls. On the other hand, drawing in of material increases with decreasing width of the blank, causing e_1 at the pole to

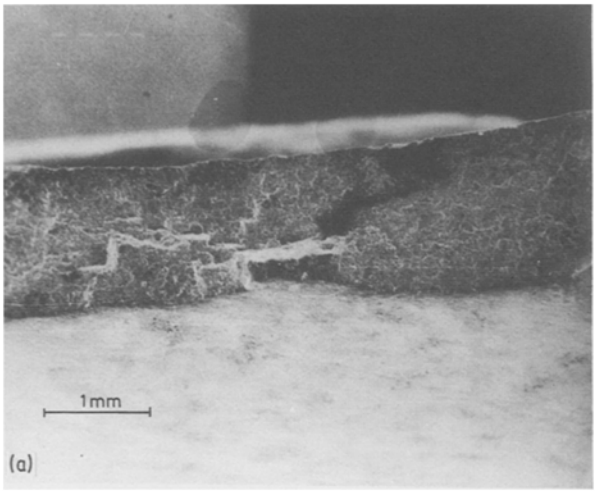

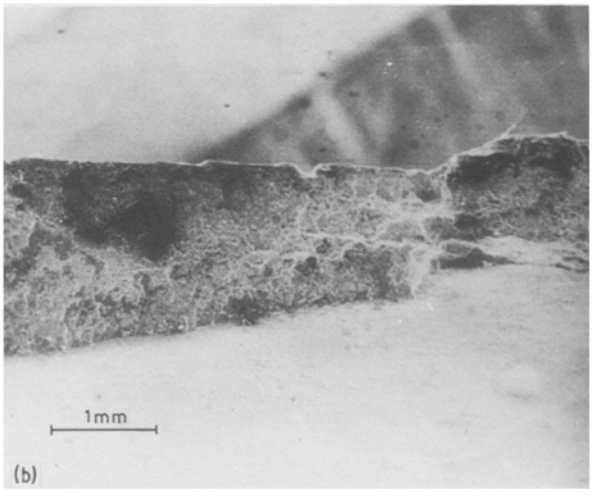

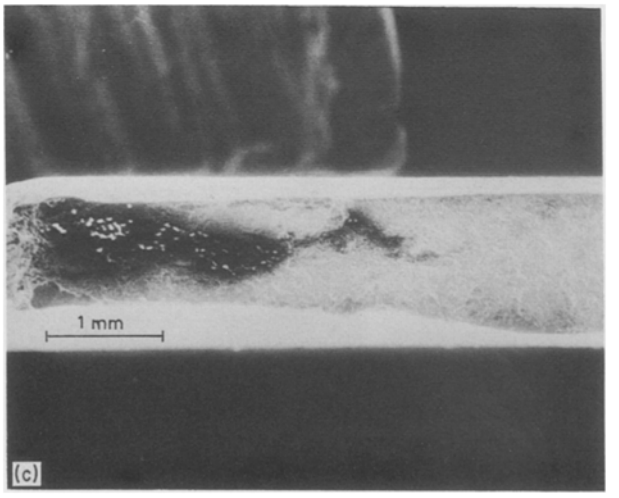

Figure 4 Tensile fracture surfaces (a) and (b) corresponding to room temperature (25° C) and cross-head speeds of 2 and 10 mm min^{-1}, respectively. (c) 190° C and a cross-head speed of 10 mm min^{-1}.

TABLE II Average dimple size for blanks of different widths

Blank width (mm)	100	60	40	25
Dimple size (μm)	4	4	4	3

rise. Then, as seen in these experiments, under identical conditions of lubrication (including no lubrication), the strain distribution (which is determined by the stress state) depends on the geometric factors such as punch profile, draw bead diameter and blank width [8].

By interpolation of the results presented in Figs 2a to h, Fig. 8 has been drawn. This way the limitation introduced by the discreteness of blank widths and non-contacting circular grids could be overcome. Evidently, Fig. 8 is a convenient way of storing data and reveals the effects of blank width and stress state on strain distribution. (Extrapolation beyond the range of blank widths employed in the experiments, however, should be avoided.)

It is clear from Fig. 8 that the effect of blank width on the (e_2/e_1) ratio is different at the pole and at 2 mm from it, compared with points further away from the pole, where the curves lie in a narrow band. The latter curves converge for a blank width of 60 mm, but are divergent above and below this value. Above a value

TABLE III Correlation between test temperature, dimple size and ductility (all measurements corresponded to a cross-head speed of 2 mm min^{-1})

Temperature (° C)	Dimple size (μm)	Total strain at fracture (%)
25	4.6	20.1
80	5.9	23.6
130	7.9	25.0
190	9.4	27.8

of 70 mm, the rise in the (e_2/e_1) ratio with blank width is less steep.

The effect of blank width on the (e_2/e_1) ratio has already been explained. It should also be noted that beyond a certain width (in this case $\sim$70 mm) the entire draw bead would have made contact with the blank and there would be no further increase in the constraints or stretching force in the e_2 direction so that the (e_2/e_1)–blank width plots flatten out.

As the radius of curvature of the punch used in this study was not large, the physical separation between distinct stress states was small. Thus, many curves in Fig. 8 lie in a narrow band. The resolution can be improved by using punches of larger radii, but then more material will be required for the tests. Alternatively, smaller grid circles could be used, in which case more accurate instruments are needed for strain measurements.

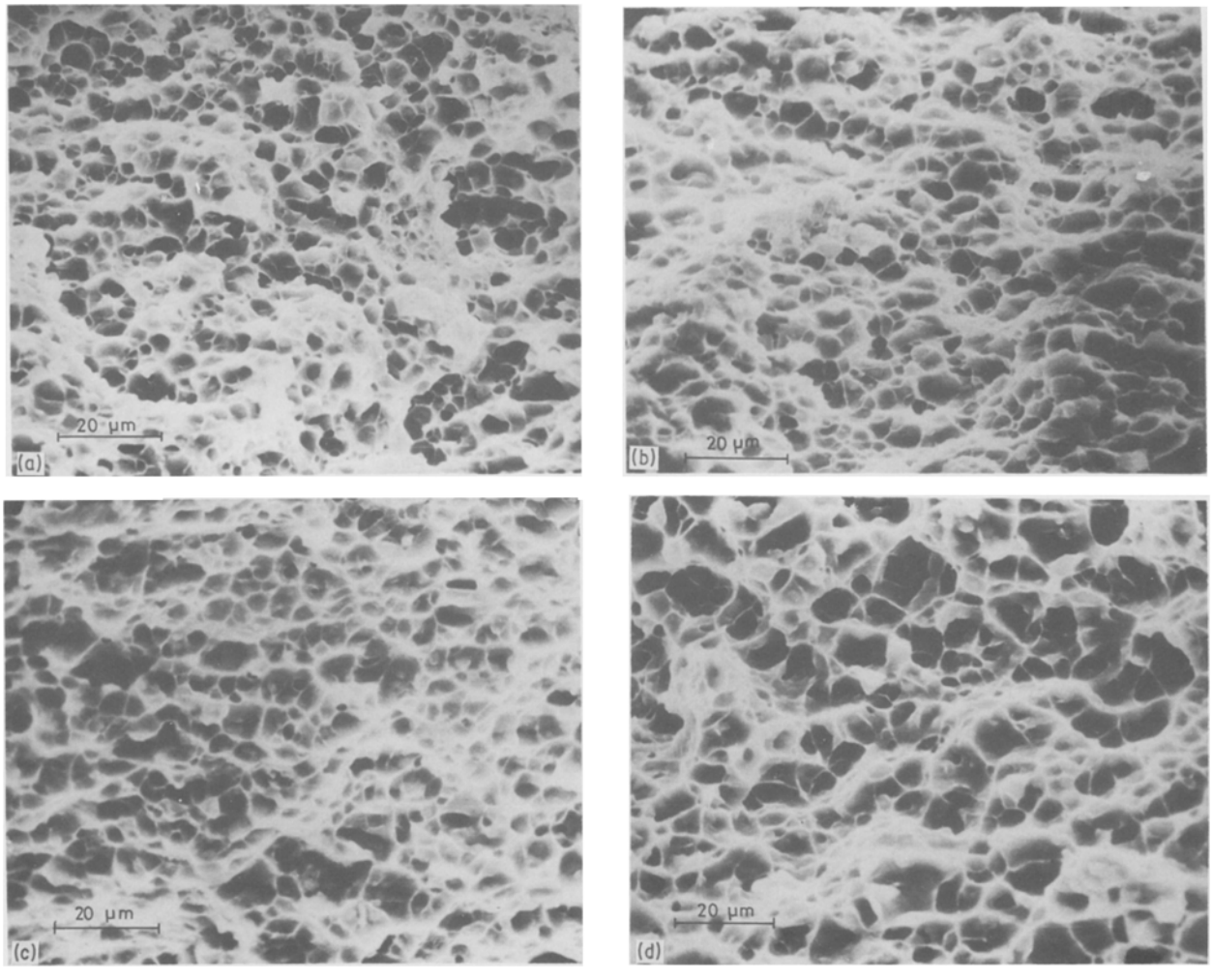

Figure 5 Dependence of dimple size on test temperature in tensile tests at a cross-head speed of 2 mm min^{-1}. (a) 25° C, (b) 80° C, (c) 130° C, (d) 190° C.

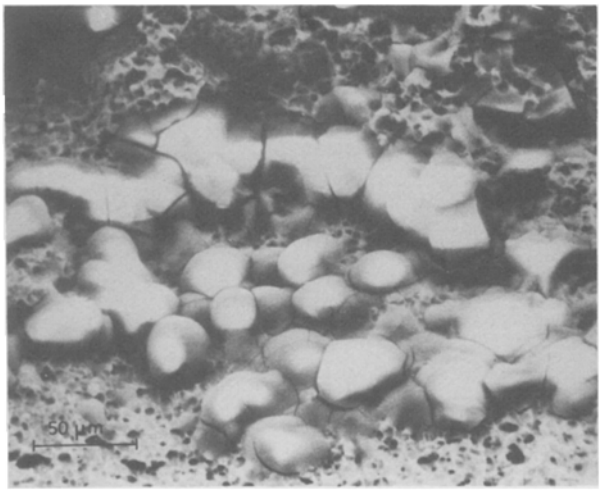

Figure 6 Evidence for the presence of grain-boundary sliding. Tensile test at 190° C and a cross-head speed of 10 mm min^{-1}.

Thus, the nature of the curves depicting the strain state is influenced by the punch to grid circle diameter ratio, blank width to bead diameter ratio and lubrication. (In this study, only the blank width to bead diameter ratio was varied.) Evidently, this aspect of the study is useful in knowing the extent of ductility available when the material is subjected in service at room temperature to different stress states. In particular, unlike the case of highly ductile materials [9], the FLD of the Al–Ca–Zn alloy in the positive e_1–e_2 space does not rise steeply, which indicates that the stress state affects ductility only marginally. The overall ductility level (at room temperature) for all stress states is limited.

4.2. Tensile properties

The effects of strain, strain rate and temperature on tensile ductility are similar to what is seen in many systems. This aspect needs no further discussion. In this material, yield-point elongation was present. Therefore, both the lower and (initial) upper yield points have been reported. The strain-hardening index (n) was calculated in the range beyond yield-point elongation up to maximum load. At the higher temperatures, the lower yield point was of the order of the UTS. (As n decreased with increasing temperature, the load maximum was seen practically at the beginning of flow.)

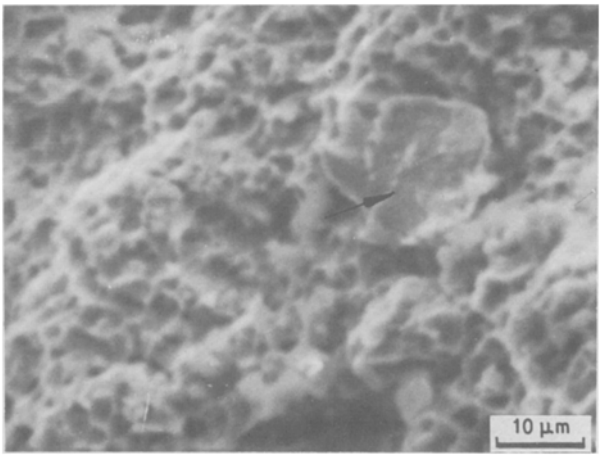

Figure 7 A shear facet (indicated by an arrow) seen in a blank of width 100 mm, fractured at room temperature by punch stretching.

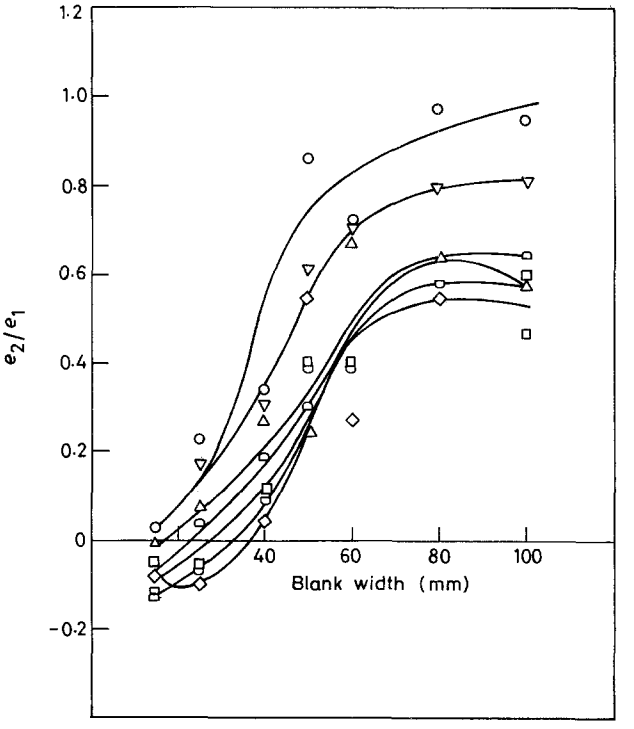

Figure 8 Dependence of the (e_2/e_1) ratio on blank width, at fixed distances (mm) from the pole (○) (▽) 2, (△) 4, (□) 6, (◇) 8, (⌣) 10, (⌓) 12.

From Table I, it is possible to choose a safe operating stress at a given temperature, by assuming a suitable factor of safety.

4.3. Fractography

In fracture induced by punch stretching, the dimple size was not affected much by the blank width, which could be traced to the limited effect of the stress state on ductility. The small differences in ductility are perhaps due to the known dependence of crack initiation and propagation on stress state.

In this alloy, cracks initiate by the fracturing of inclusions and/or by decohesion along a particle–matrix interface [6]. The width of tear ridges decreased with increasing ductility because sudden failure by plastic deformation (which leads to tearing) that connects different fracture paths becomes less important when greater crack lengths can be tolerated on account of enhanced ductility. With increasing temperature, the strain-rate sensitivity index (m) also increases (see above). This increases the internal necking resistance of intercavity ligaments, which again will decrease the tendency for tearing.

4.4. Failure criterion

As fracture first appears perpendicular to the direction of major strain, a longitudinal traverse reveals the limiting strain distribution obtainable in a blank. Therefore, for verifying the hypotheses regarding the onset of fracture, longitudinal traverses (to estimate strain) should be employed.

Marciniak *et al.* [4, 5] have postulated that an inhomogeneity lying perpendicular to the direction of greatest principal stress develops into a groove,

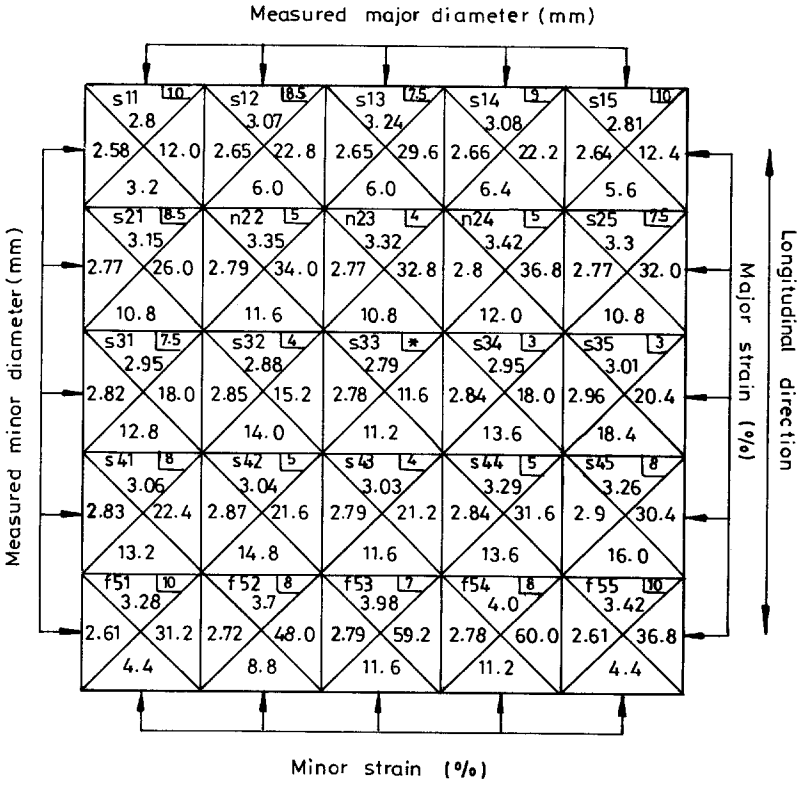

Figure 9 The major and minor strains near the pole in a punch-stretched blank of width 50 mm. Each square represents an ellipse (see text).

in which deformation becomes concentrated (leading to fracture), once a condition of plane strain, i.e. $de_2 = 0$, is reached.

This hypothesis could be verified in blanks of different widths. The procedure is illustrated in Fig. 9, which corresponds to a blank width of 50 mm. In the figure, an ellipse is represented by a square, with the one at the pole denoted by a star. The distance (mm) from the pole of other ellipses is shown in the boxes. The squares are numbered in the "row × column" notation and the symbols s, n and f are used to denote the "safe", "necked" and "fractured" ellipses. Each square is divided into four quarters. The "northern" and "eastern" quarters give, respectively, the length of the major axis (mm) and the percentage major strain. The "western" and "southern" quarters present the length of the minor axis (mm) and percentage minor strain, in that order.

The following points can be made about the minor strain gradient.

(a) Within an experimental accuracy of ± 1%, the minor strain experienced by the necked ellipses n22, n23 and n24 was identical. The safe ellipses s12, s13 and s14 (present adjacent to the necked ellipses) have also suffered an equal (but lower) minor strain.

(b) In column s13 to f53, representing a longitudinal traverse through the pole, the minor strain at the pole is 11.2%, which increased to 11.6% at s43. This value is unaltered at f53 and is equal to the minor strain present in n22, n23 and n24.

Thus, in the above cases, $de_2 = 0$ (i.e. minor strain is constant), when necking and fracture set in. In other words, a condition of plane strain exists before failure (which verifies the postulate of Marciniak *et al.* [4, 5]).

The horizontal row on either side of f53, on the other hand, emphasizes the need for stopping a test immediately on reaching the limit strain to prevent crack propagation into regions of low strain.

Thus, a single limiting minor strain (e_{2l}) could be associated with the fractured ellipses corresponding to each blank width (Fig. 10a). The reason for the increase in the limiting minor strain with blank width

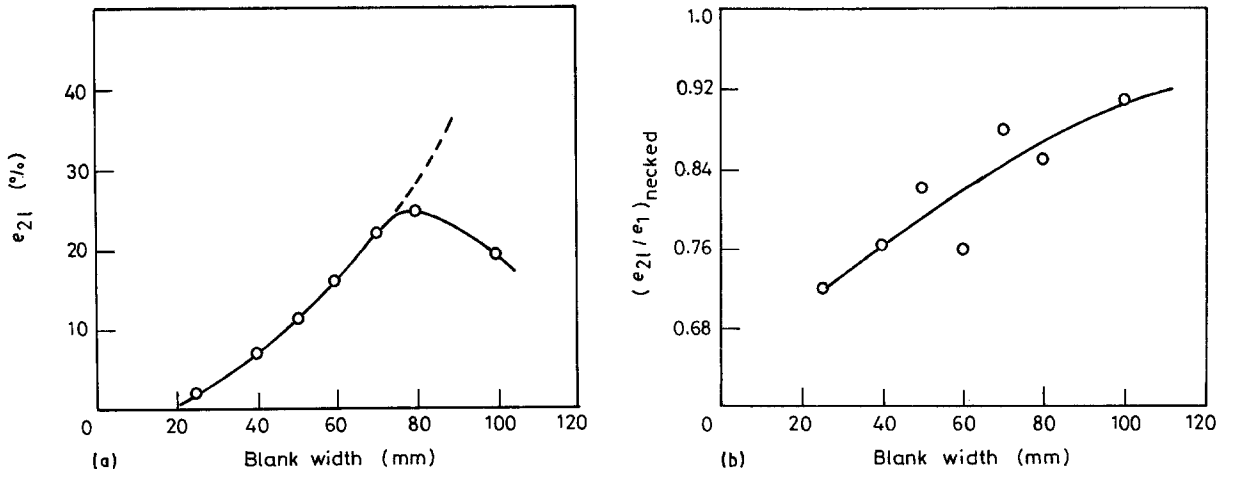

Figure 10 (a) Limiting minor strain (e_{2l}) in fractured ellipses corresponding to different blank widths. (b) The lowest (e_{2l}/e_1) ratio at the necked ellipses plotted against blank width.

and its saturation above about 70 mm has already been given. In Fig. 10b, (e_{2l}/e_l) values of necked ellipses having the largest possible e_l value and an e_{2l} value equal to that of a fractured ellipse (Fig. 10a) are plotted against the blank width. An equi-biaxial strain state $(e_{2l}/e_l = 1)$ is approached for large blank widths. For reasons already stated, the tendency slows down above a blank width of 70 mm and the presence of limited lateral drawing prevents a value of unity from being reached.

5. Conclusions

The following conclusions emerged from the present study.

1. At room temperature, more ductility was present in bi-axial than in uni-axial tension. Tensile ductility in the range room temperature (25° C) to 190° C was reasonable.

2. Plots of (e_2/e_1) against blank width could be used to store conveniently formability data corresponding to different stress states. Interpolation overcomes the problem of discreteness in blank width and non-contacting grid circles. The strain distributions, measured in longitudinal traverses, are accounted for in terms of the punch profile and the change in the extent of clamping with blank width.

3. Work-hardening capacity of the material is limited and Table I indicates that the alloy is of medium strength.

4. The tensile and fractographic results are similar to those reported for a number of systems.

5. The results verify the postulate of Marciniak *et al.* [4, 5] that fracture is first seen only after a condition of plane strain is reached.

Acknowledgements

The authors thank Dr D. M. Moore for the supply of the alloy sheets used in this study. They are grateful to Mr C. R. Prasad and Dr S. L. Mannan for allowing the use of the Instron machine.

References

1. D. M. MOORE and L. R. MORRIS, *Mater. Sci. Engng* **43** (1980) 85.
2. S. P. KEELER and W. A. BACKOFEN, *Trans. Amer. Soc. Met.* **56** (1963) 25.
3. S. S. HECKER, *Sheet Metal Ind.* **52** (1975) 671.
4. Z. MARCINIAK and K. KUCZYNSKI, *Int. J. Mech. Sci.* **9** (1967) 609.
5. Z. MARCINIAK, K. KUCZYNSKI and T. POKORA, *ibid.* **15** (1973) 789.
6. K. A. PADMANABHAN, J. HIRSCH and K. LÜCKE, unpublished work.
7. K. A. PADMANABHAN and G. J. DAVIES, "Superplasticity" (Springer Verlag, Berlin, Heidelberg and New York, 1980) pp. 30–34, 75.
8. A. K. GHOSH and S. S. HECKER, *Metall. Trans.* **5** (1974) 2161.
9. K. SWAMINATHAN, K. A. PADMANABHAN and K. S. SUBRAMANIAN, Proceedings International Conference "Advances in Metal Forming" (American Society Met. International, India Chapter, Bombay, 1987) in press.

Received 26 May
and accepted 24 July 1987